UC Irvine
UC Irvine Previously Published Works

Title
Effects of Segment Chemistry on Mechanical Performance and Hemocompatibility in Polyurethane Heart Valve Scaffolds

Permalink
https://escholarship.org/uc/item/9dr505jb

Journal
Journal of Materials Chemistry B

ISSN
2050-750X

Authors
Sadeghi, Farhad
Zamani, Yasaman
Tacklind, Mia
et al.

Publication Date
2026-10-28

DOI
10.1039/d6tb01865c

Copyright Information
This work is made available under the terms of a Creative Commons Attribution-NonCommercial-NoDerivatives License, available at https://creativecommons.org/licenses/by-nc-nd/4.0/

Peer reviewed

eScholarship.org Powered by the California Digital Library
University of California

Journal of Materials Chemistry B

ROYAL SOCIETY OF CHEMISTRY

PAPER

Published on 29 September 2026
Licence and permissions



Cite this: DOI: 10.1039/d6tb01865c

Effects of segment chemistry on mechanical performance and hemocompatibility in polyurethane heart valve scaffolds

Farhad Sadeghi, †[a] Yasaman Zamani, †[a] Mia Tacklind,[a] Robert Edwards,[b] Dan Simionescu [c] and Arash Kheradvar *[ad]

Polycarbonate-based and polysiloxane-modified thermoplastic polyurethanes (TPUs) are promising candidates for cardiovascular implants because of their tunable mechanical properties and favorable biocompatibility. In this study, we established comparative formulation–property–hemocompatibility criteria for polymeric heart valve scaffolds through a systematic evaluation of five commercial TPU formulations: carbothane AC-4095A (CB95-AC), carbothane AC-4075A (CB75-AC), carbothane PC-3575A (CB75-PC), chronoflex C65D (CF), and quadrasil ARCS 90A (Qsil). This comparative analysis provides practical material-selection criteria based on the balance between elastic recovery, tear resistance, oxidative stability, and hemocompatibility. CF and CB95-AC exhibited the highest stiffness and tensile strength, whereas CB75-AC and CB75-PC demonstrated greater elasticity and lower residual strain during cyclic loading. CB75-AC exhibited the lowest hysteresis and best elastic recovery; however, it also exhibited low tear resistance and slightly elevated hemolysis (~4%), highlighting the tradeoff between elastic recovery and mechanical robustness. All TPU materials maintained platelet counts and partial thromboplastin time values within ASTM-defined acceptable ranges. FTIR analysis revealed formulation-dependent differences in urethane carbonyl hydrogen bonding and hard-domain association that were associated with differences in mechanical behavior and surface characteristics. DSC revealed formulation-dependent differences in thermal transitions, whereas WAXD showed broadly similar, predominantly amorphous structures with diffuse scattering centered at approximately 20–21° 2θ and no distinct crystalline reflections. Preliminary short-term implantation of a CB95-AC polymeric mitral valve in an ovine model showed no gross thrombotic attachment on the leaflet surfaces after 22 days. Overall, the results demonstrate formulation-dependent tradeoffs among elastic recovery, tear resistance, oxidative stability, and hemocompatibility in TPU-based heart valve scaffolds. These findings provide practical material-selection criteria for future polymeric heart valve scaffold development.

Received 4th August 2026,
Accepted 27th September 2026

DOI: 10.1039/d6tb01865c

rsc.li/materials-b

1. Introduction

Heart valve replacement remains the standard treatment for patients with severe valvular disease. Currently, two types of prosthetic valves—mechanical heart valves (MHVs) and bioprosthetic heart valves (BHVs)—are widely used in clinical practice. MHVs, constructed from rigid materials such as pyrolytic carbon, exhibit excellent durability and long-term mechanical stability, making them suitable for younger patients. However, their use requires lifelong anticoagulation therapy to prevent thromboembolic complications, which is associated with bleeding risks and reduced quality of life.[1] In contrast, BHVs, typically made from porcine or bovine pericardial tissue, offer superior hemodynamic performance and lower thrombogenicity, often eliminating the need for anticoagulation. Despite these advantages, BHVs—including both transcatheter and surgical—are prone to calcification, structural degeneration, and limited durability, particularly in younger patients.[2,3]

These limitations have motivated the development of alternative valve technologies that can simultaneously provide long-term durability and favorable hemocompatibility without the need for lifelong anticoagulation. In recent years, polymeric heart valves (PHVs) have gained increasing attention as a

[a] Department of Biomedical Engineering, University of California, Irvine, USA. E-mail: arashkh@uci.edu; Fax: +1 949-725-2891; Tel: +1 949-824-6538
[b] Department of Pathology & Laboratory Medicine, University of California, Irvine, USA
[c] Department of Bioengineering, Clemson University, Clemson, USA
[d] Department of Radiological Sciences, University of California, Irvine, USA
† Shared first authorship, Farhad Sadeghi and Yasaman Zamani contributed equally to this manuscript.

potential alternative to MHVs and BHVs. Advances in polymer chemistry and processing have enabled the development of materials that combine mechanical robustness, flexibility, and hemocompatibility essential for a heart valve. These valves aim to combine the durability of MHVs with the hemodynamic and biocompatible advantages of BHVs, thereby reducing the need for lifelong anticoagulation or repeat surgeries.[4] However, despite encouraging progress, most PHV designs remain limited by poor bioactivity[5] and a susceptibility to calcification,[6] thrombosis,[7] and immune responses[8] after implantation. These challenges highlight the need for materials that not only exhibit mechanical resilience but also promote favorable biological interactions at the blood–material interface.

To address these challenges, combining tissue-engineering principles with polymer scaffolds has emerged as a promising approach; integrating living cells and extracellular matrix (ECM) components onto a nondegradable polymeric valve framework to promote *in situ* regeneration and remodeling. Building on this concept, our group has introduced the concept of hybrid tissue-engineered heart valves (H-TEHVs) that unite the biological functionality of living tissue with the mechanical durability of a nondegradable synthetic scaffold.[9–12] In this approach, a robust polymeric scaffold is coated with autologous cells to replicate native valvular microarchitecture, thereby promoting endothelialization and reducing adverse host responses. This approach also overcomes the mechanical instability and scaffold degradation commonly associated with traditional tissue-engineered heart valves (TEHVs), while eliminating the need for long-term anticoagulation therapy. Ongoing efforts are focused on optimizing the composition and performance of the polymeric scaffold for this platform.

Among candidate materials, polycarbonate-based thermoplastic polyurethanes (PC-TPUs) have emerged as particularly promising due to their segmented microstructure, which enables independent tuning of elasticity, strength, and surface properties. Their soft segments provide flexibility and extensibility, while hard segments act as physical crosslinks that govern mechanical stability and durability.[13] In addition, polycarbonate-based polyurethanes have demonstrated improved oxidative stability compared to polyether-based polyurethanes, making them attractive for long-term cardiovascular applications. Nevertheless, a systematic understanding of how differences among TPU chemistry classes and their associated formulation characteristics relate to mechanical performance and hemocompatibility remains incomplete, particularly in the context of heart valve scaffold selection.

In our previous study,[14] we characterized PC-TPUs as potential scaffold materials, assessing cytotoxicity, surface morphology, and cell attachment. The present work extends this effort by systematically evaluating selected PC-TPU formulations as candidates for polymeric heart valve scaffolds. To our knowledge, this is the first study to establish comparative material-selection criteria for PC-TPUs based on elastic recovery, tear resistance, oxidative stability, surface characteristics, and *in vitro* hemocompatibility, all of which are essential considerations for heart valve scaffold performance. Although several individual structure–property relationships of TPUs are well established, their combined implications for heart valve scaffold selection remain insufficiently defined. The present study therefore focuses on the integrated assessment of competing performance requirements rather than optimization of any single material property, with the goal of identifying formulation-specific tradeoffs relevant to polymeric heart valve scaffold selection.

This work is designed as a material-level screening study of TPU-based polymeric scaffold candidates for future heart valve applications. Although these materials are intended for eventual use in hybrid tissue-engineered heart valve platforms, the current study focuses on their material properties rather than tissue-engineering function. Tissue-engineering outcomes, including cell attachment, endothelialization, ECM deposition, inflammatory response, and remodeling behavior, are being investigated in a separate study and are beyond the scope of the present work. Therefore, the findings should be interpreted as comparative scaffold material-screening data rather than full validation of tissue-engineered valve function.

We hypothesized that differences in overall TPU formulation and resulting microphase organization would produce distinct balances among elastic recovery, tear resistance, oxidative stability, and hemocompatibility. Through this analysis, we aimed to identify formulation–property–function relationships and establish practical material-selection criteria for mechanically robust and hemocompatible candidate materials for future polymeric heart valve development, including next-generation H-TEHV applications.

2. Materials and methods

2.1. Materials preparation and characterization

Five polycarbonate-based thermoplastic polyurethane (TPU) resins were evaluated in this study: carbothane AC-4095A, carbothane AC-4075A, carbothane PC-3575A (Lubrizol), chronoflex C 65D (AdvanSource), and quadrasil ARCS 90A (Biomerics). These materials were selected as candidate formulations representing different commercial TPU families, including aromatic and aliphatic PCUs and a polysiloxane-modified PCU, across a range of nominal hardness values. Hereafter, these materials are referred to as CB95-AC, CB75-AC, CB75-PC, CF, and Qsil, respectively as summarized in Table 1. The chemistry classifications summarized in Table 1 are based on available manufacturer information and represent the major formulation families evaluated in this study. Because these are proprietary commercial materials, the

Table 1 Description of polycarbonate-based thermoplastic polyurethanes

Material	Abbreviation	Chemistry	Hardness
Carbothane AC-4075A	CB75-AC	Aromatic PCU TPU	~75A
Carbothane AC-4095A	CB95-AC	Aromatic PCU TPU	~95A
Carbothane PC-3575A	CB75-PC	Aliphatic PCU TPU	~70A
ChronoFlex C 65D	CF	Aromatic PCU TPU	65D
Quadrasil ARCS 90A	Qsil	Silicone-PCU copolymer	~90A

This journal is © The Royal Society of Chemistry 2026

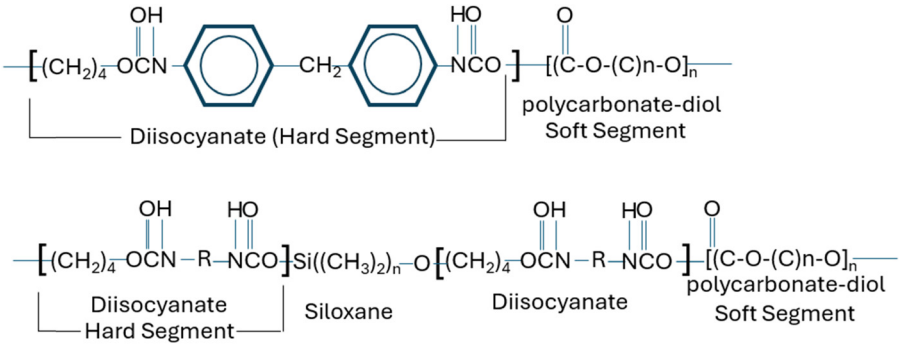


Fig. 1 Chemical structure of polycarbonate-based and polysiloxane-modified thermoplastic polyurethanes (TPUs). The molecular structure of TPU comprises three main segments: (1) isocyanate, (2) polyol, which may be polyester, polyether, or polycarbonate, and (3) a chain extender. The reaction of these components forms a morphology known as a segmented structure, including alternating soft and hard segments. The combination of the chain extender and diisocyanate forms the hard segments, while the polyol component forms the soft segments.

present analysis focuses on formulation-level comparisons supported by experimentally measured rheological, mechanical, FTIR, surface, and hemocompatibility characteristics rather than isolation of individual molecular constituents (Fig. 1).

2.2. Rheological characterization

Rheological and mechanical characterization was performed at the TEMPR facility at the University of California, Irvine. Rheological measurements were obtained using a Discovery Series Hybrid Rheometer HR-2 (TA Instruments, New Castle, DE). Viscosity–frequency sweep tests were conducted in oscillatory mode at 200 °C for melt samples and at room temperature for solution samples. Strain sweep tests were first performed to confirm that all measurements were acquired within the linear viscoelastic region.

Polymer films were prepared from polymer solutions for mechanical testing. Sheets were developed by solution casting, in which resin granules were dissolved in dimethylacetamide (DMAc) at 60 °C for 24 h to obtain a 20 wt% solution. The solutions were poured into a rectangular mold and dried in an oven at 60 °C for 6 hours, yielding sheets with an average thickness of ∼80 μm. All films were visually inspected to ensure uniformity and absence of defects prior to testing. For melt-processed specimens, resins were compression-molded at 220 °C for 8 min and cooled to room temperature.

2.3. Dynamic mechanical analysis

Dynamic mechanical analysis (DMA) was performed using a DMA Q800 (TA Instruments, New Castle, DE) in tension mode to assess the stiffness of solution-cast sheets. Samples were tested at a strain amplitude of 0.1% frequency of 2 to 100 rad s^{-1} and temperature condition of 22 °C isothermal. Storage modulus and tan δ were recorded under these conditions. This frequency range was selected as a standard DMA material-characterization approach to compare the relative viscoelastic responses of the TPU formulations under controlled testing (liner viscoelastic region) conditions, rather than directly reproducing heart valve leaflet cycling.

2.4. Fourier transform infrared spectroscopy (FTIR)

FTIR spectra were acquired using a Nicolet Apex FTIR spectrometer (Thermo Fisher Scientific, WI) with a resolution of 4 cm^{-1} and 16 co-added scans. Spectra were collected over an appropriate wavenumber range to capture characteristic functional group vibrations.

To evaluate oxidative degradation following accelerated aging, chemical changes were monitored by analyzing the carbonyl stretching region. The integrated carbonyl absorbance (1700–1735 cm^{-1}) was normalized to the methylene (–CH_2–) peak at 2860 cm^{-1} to account for variations in sample thickness. The resulting carbonyl ratio was used as a semi-quantitative indicator of oxidative damage.[15] The carbonyl hydrogen-bonding state was evaluated using the method described by Huang *et al.*[16] based on deconvolution of the carbonyl stretching region. Specifically, two characteristic bands were analyzed: (i) a higher-wavenumber peak associated with non–hydrogen-bonded ("free") urethane C═O stretching and (ii) a lower-wavenumber peak attributed to hydrogen-bonded urethane carbonyls (C═O···H–N), which are enriched within hard domains. The carbonyl region was baseline-corrected and analyzed in absorbance mode using PeakFit software. The overlapping carbonyl bands were deconvoluted using Gaussian peak functions, and the fitted absorbance heights of the hydrogen-bonded and free carbonyl components were used to calculate the hydrogen-bonded/free carbonyl absorbance-height ratio. This ratio was used as a semi-quantitative indicator of relative urethane carbonyl hydrogen bonding and hard-domain association among the formulations.

2.5. Differential scanning calorimetry (DSC)

Differential scanning calorimetry (DSC) was performed at the TEMPR facility at the University of California, Irvine, using a DSC 2500 (TA Instruments, New Castle, DE) to evaluate the thermal behavior of the TPU films. Samples were heated from −70 °C to 200 °C at a rate of 10 °C min^{-1}. The heating cycles for the samples were compared to assess formulation-dependent thermal transitions.

2.6. Wide-angle X-ray diffraction (WAXD)

Wide-angle X-ray diffraction (WAXD) analysis was performed at the TEMPR facility at the University of California, Irvine, using a Rigaku SmartLab X-ray diffractometer to evaluate the structural organization of the TPU films. Samples were analyzed in Bragg–Brentano θ–2θ geometry using Cu Kα radiation at 40 kV and 44 mA over a 2θ range of 3–90°, with a step size of 0.02° and a scan rate of 4° min^{-1}. The diffraction patterns were compared to assess formulation-dependent differences in structural ordering and crystallinity. For comparison in the manuscript, the normalized diffraction profiles are presented over the 5–40° 2θ range, encompassing the principal polymer-associated scattering features.

2.7. Accelerated aging

Accelerated aging was performed to simulate *in vivo* oxidative conditions by exposing film samples to a solution of 0.1 M $CoCl_2$ and 20% H_2O_2 in deionized water at room temperature for 30 days.[17] After exposure, samples were thoroughly rinsed with deionized water and dried prior to further analysis. Oxidation was quantified by tracking the increase in carbonyl absorbance within the 1700–1735 cm^{-1} region using FTIR. To account for variations in film thickness and sampling, the integrated carbonyl absorbance was normalized to the intensity of the methylene (–CH_2–) peak at 2860 cm^{-1}, which remains stable under oxidative conditions. The resulting carbonyl ratio provides a semi-quantitative measure of oxidative damage and enables comparison of relative degradation across samples.[15] Following aging, samples were mechanically tested under wet conditions at 37 °C unless otherwise specified.

2.8. Tensile, hysteresis, and tear tests

Tensile and hysteresis tests were performed using an Instron 3365 dual-column universal testing system (Norwood, MA) at a crosshead speed of 100 mm min^{-1}, with a gauge length of 25 mm and a sample width of 15 mm.

Cyclic hysteresis testing over 100 cycles was used to evaluate the short-term cyclic mechanical response, elastic recovery, and resistance to permanent deformation of the TPU films under 10% strain. These tests were not intended to represent long-term valve fatigue durability, which will require accelerated valve-level testing. Rather, the purpose of this test was to provide comparative information on the strain-recovery behavior and hysteresis response of the polymer formulations under identical cyclic loading conditions.

Tear testing was performed on 25-mm-wide specimens containing a 15 mm pre-cut notch using a tensile testing machine. The notch was propagated under uniaxial tensile loading at a speed of 500 mm min^{-1} until complete failure. The maximum force applied before rupture was recorded and reported as the tear resistance. Three measurements were performed for each sample, and the results are reported as the average value ± standard deviation. Hysteresis tests were performed at a stretching speed of 100 mm min^{-1} with a 25 mm gauge length. Stress–strain curves were recorded, and the residual strain remaining in the samples was measured at two strain amplitudes: 10% normal strain and 50% large strain. These tests were used to analyze the material response under different levels of strain.

2.9. Contact angle

Static water contact angle measurements were acquired using an MSE PRO entry-level contact angle goniometer (Model MA211; Tucson, AZ) on the surfaces of the samples. Three measurements were performed for each sample, and the results are reported as the average value ± standard deviation.

2.10. Hemocompatibility evaluation

Platelet count assay: platelet count was assessed in accordance with ASTM F2888-19 for evaluating thrombogenic potential of blood-contacting materials. Briefly, TPU samples and control materials were prepared in triplicate at a surface area-to-blood volume ratio of 12 cm^2 mL^{-1} and placed in polypropylene tubes. Fresh human whole blood, anticoagulated with sodium citrate, was obtained from healthy donors under UCI Institute for Clinical & Translational Science (ICTS) Normal Blood Donor Program (IRB #2001-2058) and written informed consent was obtained from all participants. Prior to exposure, blood was recalcified and supplemented with heparin as specified in the standard. Samples were incubated with blood at 37 ± 2 °C under gentle agitation (~60 rpm) for 1 h. Following incubation, EDTA was added to terminate further reactions. Blood was carefully collected, mixed, and analyzed using a DxH 520 hematology analyzer (Beckman Coulter, Brea, CA) to determine platelet counts. Each sample was measured in duplicate, and values were normalized to the negative control (blood without material exposure). Materials were considered acceptable if platelet counts remained within 80–120% of the control, in accordance with ASTM criteria.

Partial thromboplastin time (PTT) assay: coagulation activity *via* the intrinsic pathway was evaluated using a modified partial thromboplastin time (PTT) assay based on ASTM F2382-24. TPU samples were cut into dimensions of 1 × 3 cm^2 and placed in polypropylene tubes along with reference materials and controls. Each sample was incubated with 1 mL of citrated human plasma (UCI IRB protocol 20012058) at 37 ± 2 °C for 15 ± 1 min in an agitating water bath (60 rpm). Following incubation, the samples were vortexed for 15 s, and 100 μL of plasma was carefully transferred to a 96-well plate while avoiding bubble formation, followed by equilibration at 37 ± 2 °C for 60 s. Subsequently, 100 μL of pre-warmed rabbit brain cephalin (RBC) reagent was added to initiate the activation step, followed by incubation for 2 min. Clotting was triggered by the addition of 100 μL of pre-warmed 25 mM calcium chloride, and the plate was shaken for 10 s. Absorbance was monitored at 405 nm every 5 seconds for 6 min using a Varioskan LUX multimode microplate reader (Thermo Scientific, USA). Clotting time was determined as the time required to reach the midpoint between the minimum and maximum absorbance values following calcium chloride addition. All samples were tested in triplicate, and clotting times were normalized to the negative control (plasma

 This journal is © The Royal Society of Chemistry 2026

without material exposure) and expressed as a percentage of the control. Results were normalized to the negative control and expressed as a percentage, with 80–120% considered acceptable.

Hemolysis assay: hemolytic potential was evaluated based on ASTM F756-17 guidelines using a modified protocol. This test was performed using a Biomaterial Haemolytic Assay Kit (CTMM-0322-MM3, Creative Biolabs, Shirley, NY) with human erythrocyte suspensions. Cryopreserved erythrocytes were thawed at 37 °C and washed through repeated dilution and centrifugation steps using dilution buffers to remove residual plasma and stabilize the cells. The erythrocytes were resuspended in buffer to obtain a uniform suspension. Sterile TPU samples and controls were placed in microcentrifuge tubes, and 0.5 mL of erythrocyte suspension was added to each sample, ensuring complete immersion. A negative control (erythrocytes without material) and a total hemoglobin control (erythrocytes lysed in lysis buffer) were included. Samples were incubated at 37 °C under end-over-end rotation for 24 h. After incubation, samples were centrifuged ($>4000\times g$, 1 min), and supernatants were collected. Aliquots were transferred to a microplate, diluted with assay buffer, and absorbance was measured at 415 nm (Varioskan LUX, Thermo Scientific, USA). Hemoglobin concentration was determined using a calibration curve, and hemolysis was calculated as a percentage relative to total hemoglobin. Materials were classified as non-hemolytic ($<2\%$), slightly hemolytic (2–5%), or hemolytic ($>5\%$) according to ASTM guidelines.

In vivo assessment: a tri-leaflet mitral valve was prototyped using CB95-AC cast over a nitinol stent. The valve was surgically implanted in the mitral position of a 50 kg sheep through a midsternal thoracotomy using a cardiopulmonary bypass machine under the control of a perfusion team. The surgical procedure was performed according to the IACUC protocol AUP-25-109 approved by UCI. Twenty-two days after implantation, the valve and surrounding tissue were explanted and fixed in 4% paraformaldehyde for 24 hours prior to paraffin embedding. The fixed tissue blocks were sectioned and stained with hematoxylin and eosin (H&E) for histological evaluation.

2.11. Statistical analysis

Unless otherwise specified, quantitative *in vitro* experiments were performed in triplicate ($n = 3$), and results are presented as mean ± standard deviation. Statistical significance was evaluated using one-way analysis of variance (ANOVA) followed by appropriate *post hoc* tests. Differences were considered statistically significant at $p < 0.05$. All statistical analyses were performed using GraphPad Prism 11.0.1 (90).

3. Results

3.1. Rheological behavior of TPU melts and solutions

The viscosity–frequency profiles of the polyurethane melts and 20 wt% DMAc solutions are shown in Fig. 2a and b, respectively. All TPU formulations exhibited non-Newtonian shear-thinning behavior in the melt state, characterized by decreasing viscosity with increasing frequency. Qsil and CB95-AC showed the highest melt viscosities. CB75-AC showed higher melt viscosity than CB75-PC. CF exhibited lower melt viscosity than the other formulations.

In 20 wt% DMAc solution, CB75-AC and Qsil maintained shear-thinning behavior, whereas CB95-AC and CF exhibited lower viscosities and a more Newtonian-like response. Overall, CB75-AC and Qsil demonstrated the highest solution viscosities among the tested materials.

3.2. Tensile properties and elastic recovery

Tensile testing results are shown in Fig. 3a. The tensile stress at 100% strain for CF, CB95-AC, Qsil, CB75-AC, and CB75-PC was 19.7, 12, 9.4, 3.1, and 1.3 MPa, respectively. These results indicate a progressive decrease in stiffness and stress-bearing capacity from CF to CB75-PC, consistent with their relative hardness.

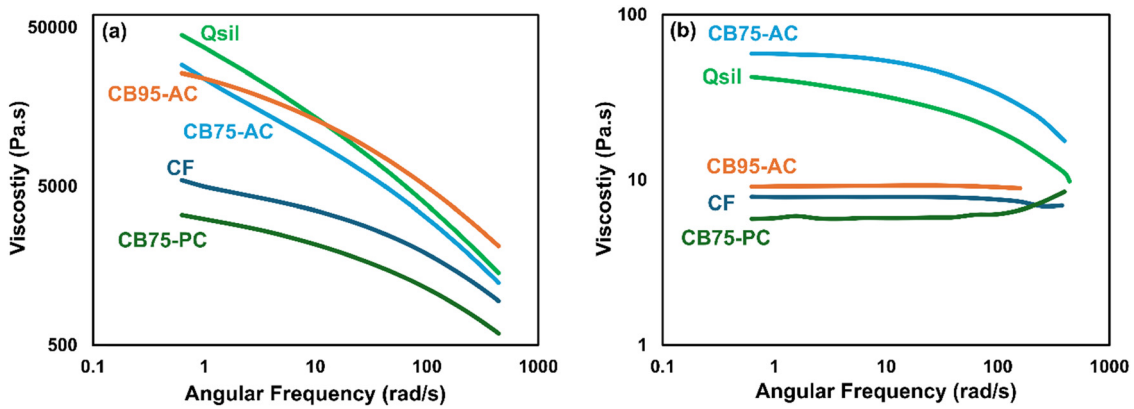


Fig. 2 Oscillatory viscometry results. (a) Viscosity–frequency sweep of TPU melts at 200 °C. All five formulations exhibited non-Newtonian shear-thinning behavior, with viscosity decreasing as frequency increased. Qsil showed the highest melt viscosity and a pronounced viscosity drop at higher frequencies. (b) Viscosity–frequency sweep of TPU samples dissolved in DMAc at 20 wt% and 25 °C. CB75-AC and Qsil displayed more pronounced shear-thinning behavior, whereas the other formulations showed more Newtonian-like behavior. CB75-PC exhibited the lowest solution viscosity.

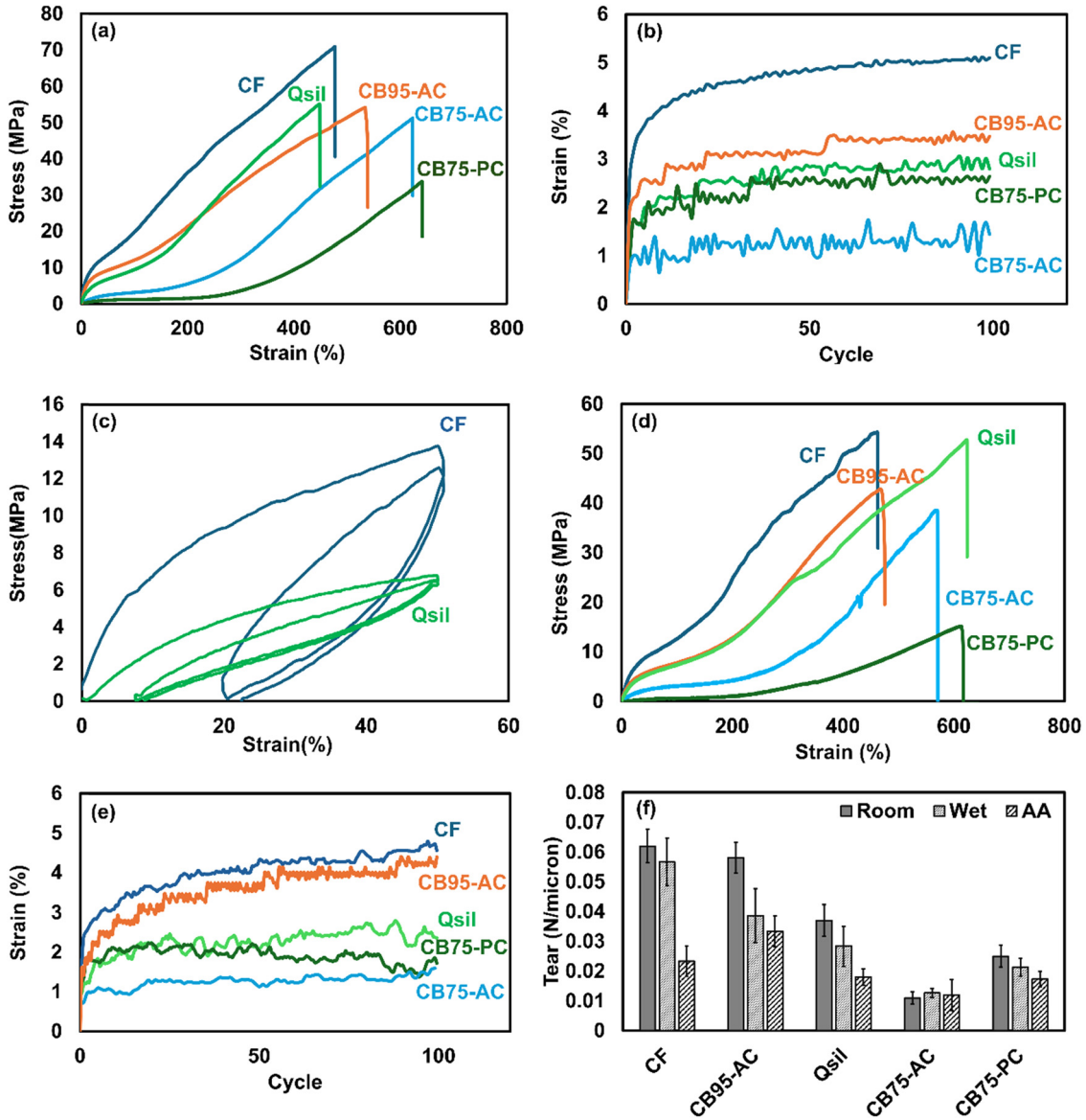


Fig. 3 Mechanical characterization of TPU films. (a) Tensile testing. CF exhibited the highest tensile stress, followed by CB95-AC, Qsil, CB75-AC, and CB75-PC. (b) Cyclic hysteresis at room temperature. CB75-AC exhibited the lowest residual strain, and all materials stabilized after approximately 100 cycles. (c) Representative cyclic stress–strain curves of CF and Qsil under large-strain loading at 50%, illustrating distinct material responses. (d) Following accelerated oxidative aging and testing at 37 °C, all formulations exhibited reduced tensile strength, although their overall mechanical profiles remained largely preserved. (e) Wet cyclic loading at 37 °C. CB95-AC became more plasticized in the presence of moisture, while CB75-AC, CB75-PC, and Qsil exhibited minimal moisture-induced changes. (f) Tear resistance decreased following both moisture exposure and accelerated oxidative aging (AA), with CF and CB95-AC exhibiting the greatest reductions, whereas CB75-AC and CB75-PC showed comparatively smaller declines in tear resistance.

Residual strain values obtained from cyclic hysteresis testing at room temperature with an applied strain limit of 10% are shown in Fig. 3b. All materials exhibited progressive stabilization of cyclic response, reaching a plateau state after approximately 100 cycles. CB75-AC showed the lowest residual strain, while CF exhibited the highest residual strain after 100 cycles. Under a larger strain amplitude of 50%, the residual strain after two loading cycles was evaluated, as shown in Fig. 3c. The residual strains for CF, CB95-AC, Qsil, CB75-AC, and CB75-PC were 22.4%, 13.4%, 8.9%, 7.2%, and 7.3%, respectively. CB75-AC and CB75-PC exhibited the lowest residual strain, indicating improved elastic recovery compared with the other formulations. Representative cyclic stress–strain curves for CF and Qsil are shown in Fig. 3c to illustrate distinct cyclic responses, while the residual strain values are reported for all materials.

3.3. Mechanical stability after accelerated oxidative aging

Stress–strain curves measured at 37 °C under wet conditions, representing physiological conditions, are shown in Fig. 3d. All materials exhibited a reduction in tensile stress after aging. The tensile stresses at 100% strain for CF, CB95-AC, Qsil, CB75-AC, and CB75-PC decreased to 12.5, 7.7, 7.3, 3.0, and 0.46 MPa,

 This journal is © The Royal Society of Chemistry 2026

respectively. Despite this reduction, the overall mechanical response profiles of the materials were preserved.

3.4. Cyclic hysteresis under physiological conditions

Residual strain values obtained from cyclic hysteresis testing under physiological conditions (37 °C, wet environment) are shown in Fig. 3e. The specimens were subject to 100 loading cycles with an applied strain limit of 10%. This test was performed to assess the combined effects of moisture and physiological temperature on the mechanical response of the films. Overall, the curves exhibited trends similar to those observed under room-temperature conditions. Notably, CB95-AC showed the most significant moisture-induced effect, with a more pronounced plastic response during cyclic loading in the wet state. CB75-AC, CB75-PC, and Qsil showed only minimal changes in cyclic behavior, suggesting that their mechanical responses were less sensitive to moisture under these conditions.

3.5. Tear resistance in dry, wet, and aged states

Tear resistance measurements under dry room-temperature, wet 37 °C, and aged wet 37 °C conditions are shown in Fig. 3f. Tear resistance varied across both material type and testing condition. In general, moisture exposure reduced tear resistance across the formulations, and further changes were observed after accelerated aging. CF and CB95-AC exhibited pronounced reductions in tear resistance following oxidative aging, whereas CB75-AC and CB75-PC showed comparatively smaller declines.

3.6. Dynamic mechanical properties of solution-cast films

The DMA results (Fig. 4a) show the storage modulus of the solution-cast polymers. The overall trend was consistent with the tensile data, with CF and CB95-AC exhibiting the highest stiffness. In contrast, Qsil showed a substantially lower storage modulus (compared to CB95-AC), followed by CB75-PC and CB75-AC. It is important to note that the storage modulus reflects the elastic response of the material under low-amplitude strain (0.1%), capturing behavior within the linear viscoelastic regime.

The tan δ results (Fig. 4b) revealed that CF exhibited the highest damping, followed by Qsil, CB95-AC, CB75-PC, and finally CB75-AC. The low tan δ of CB75-AC indicates a more elastic response and improved recovery at small strain amplitudes. In general, a higher tan δ corresponds to greater energy dissipation within the material, reflecting increased viscoelastic damping.

3.7. Hard-segment interactions and oxidation by FTIR

FTIR spectroscopy results are presented in Fig. 5. The analysis revealed notable differences in the carbonyl absorption peaks at 1700 and 1735 cm^{-1} among the formulations. The hydrogen-bonded/free carbonyl absorbance-height ratios for CF, CB95-AC, Qsil, CB75-AC, and CB75-PC were 0.54, 0.46, 0.48, 0.45, and 0.26, respectively. These results indicate that CB75-PC exhibits the lowest relative hydrogen-bonded/free carbonyl ratio among the tested formulations, corresponding to a lower relative extent of urethane carbonyl hydrogen bonding and a greater contribution from free C═O stretching vibrations.

FTIR analysis was also performed on accelerated-aged samples to assess oxidative effects. The oxidation index was defined as the integrated carbonyl absorbance in the 1700–1735 cm^{-1} region, normalized to the methylene ($-CH_2-$) peak at 2860 cm^{-1}, which remains stable under oxidative conditions and serves as a reference. The resulting oxidation indices for CF, CB95-AC, Qsil, CB75-AC, and CB75-PC—expressed as percent increase relative to the original samples—were 2.7, 2.8, 9.8, 4.7, and 6.7, respectively. This increase in carbonyl content provides a semi-quantitative measure of surface oxidation while accounting for variations in sample thickness and measurement conditions.[15]

3.8. Thermal transitions by differential scanning calorimetry (DSC)

DSC analysis showed distinct formulation-dependent thermal responses (Fig. 6). CB75-AC and CB75-PC exhibited the most evident low-temperature transitions, broadly between approximately −35 and −20 °C, whereas the corresponding changes in CF, Qsil, and CB95-AC were more gradual. CB75-PC displayed a

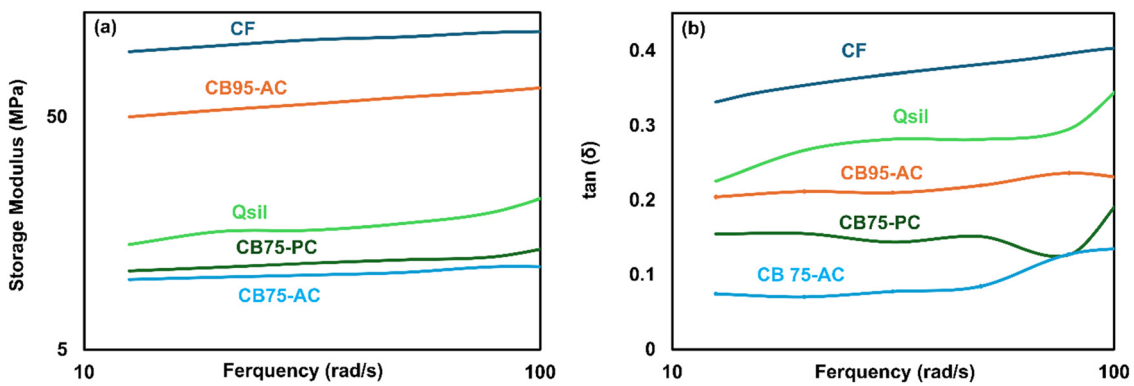


Fig. 4 Dynamic mechanical analysis (DMA) of TPU films. (a) Storage modulus measurements. CF and CB95-AC exhibited the highest stiffness, while Qsil, CB75-PC, and CB75-AC displayed progressively lower moduli under low-amplitude strain (0.1%). (b) tan δ curves. CF displayed the greatest viscoelastic damping, followed by Qsil, CB95-AC, and CB75-PC, while CB75-AC exhibited the lowest tan δ. Higher tan δ values indicate greater energy dissipation during cyclic deformation, reflecting differences in the viscoelastic behavior of the TPU formulations.

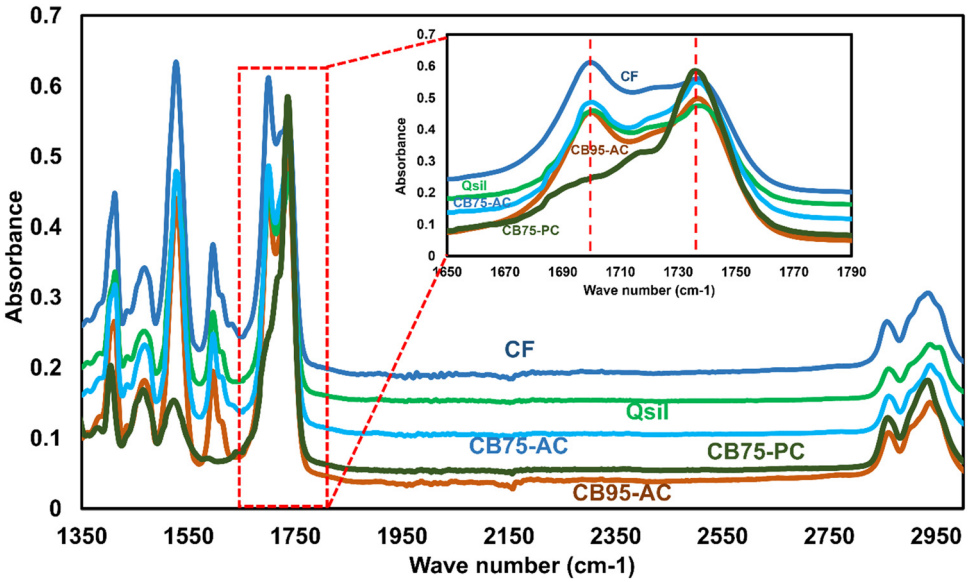


Fig. 5 FTIR spectra of TPU films. FTIR spectra showed distinct differences in the carbonyl absorption peaks at ~1735 cm^{-1} (free C═O) and ~1700 cm^{-1} (hydrogen-bonded C═O), reflecting formulation-dependent differences in urethane carbonyl hydrogen bonding. A higher proportion of hydrogen-bonded carbonyls indicates a greater relative extent of urethane carbonyl hydrogen bonding and hard-domain association. Among the samples, CB75-PC exhibited the lowest relative hydrogen-bonded carbonyl contribution.

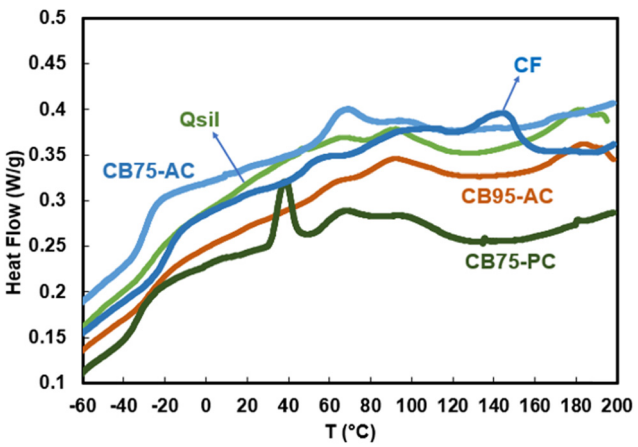


Fig. 6 Differential scanning calorimetry (DSC) thermograms of TPU films: CB75-AC and CB75-PC exhibited the most pronounced low-temperature transitions, while Qsil, CB95-AC, and CF showed more gradual changes in this region. CB75-PC displayed a distinct thermal event near 40 °C, CB75-AC showed a broader transition near 65–70 °C, and Qsil and CB95-AC exhibited broader features in the approximately 70–100 °C range. CF showed an additional pronounced higher-temperature transition near 145–150 °C, highlighting formulation-dependent differences in the thermal organization of the TPU materials.

distinct sharp thermal event near 40 °C, while CB75-AC exhibited a broader transition centered near 65–70 °C. Qsil and CB95-AC showed comparatively broad, gradual features in the approximately 70–100 °C region. In contrast, CF exhibited an additional pronounced higher-temperature transition near 145–150 °C. Overall, the DSC profiles were dominated by broad formulation-dependent thermal transitions rather than well-defined high-temperature melting peaks, indicating differences in thermal and segmental organization among the TPU formulations.

3.9. Structural organization by wide-angle X-ray diffraction (WAXD)

WAXD analysis showed broadly similar diffraction profiles among the five TPU formulations (Fig. 7). All materials exhibited a broad diffuse scattering halo centered at approximately 20–21° 2θ, with no distinct sharp polymer crystalline reflections, indicating predominantly amorphous structures with limited long-range crystalline ordering. Minor differences in the breadth and shape of the scattering profiles were observed among the formulations.

3.10. Surface wettability of TPU films

Contact angle measurements for the solution-cast films are presented in Fig. 8. Overall, all TPU formulations exhibited relatively comparable contact angle values, indicating similar surface wettability among the materials. However, CB75-PC showed a moderately higher contact angle compared to the other formulations, consistent with the relatively more hydrophobic character commonly associated with aliphatic polyurethane structures and lower surface polarity.

3.11. Hemocompatibility assessment of TPU films

Hemocompatibility of the TPU films was assessed through platelet count, coagulation response, and hemolysis assays (Fig. 9). All tested TPU samples exhibited platelet counts within the acceptable range of 80–120% relative to the whole-blood negative control (Fig. 9a), indicating no significant platelet consumption under the test conditions. Similarly, partial

 This journal is © The Royal Society of Chemistry 2026

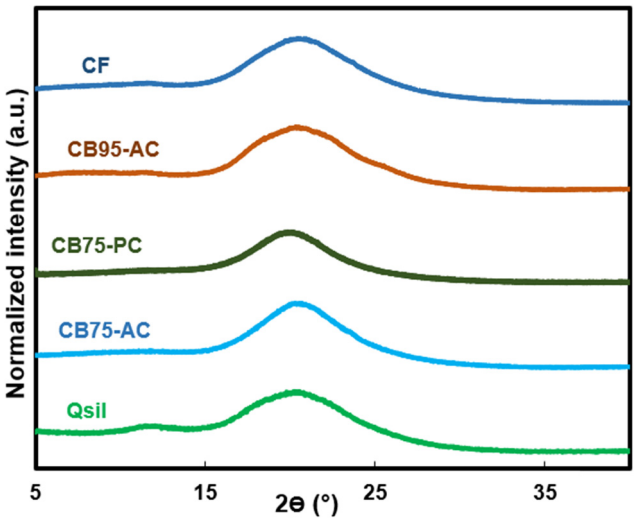


Fig. 7 Wide-angle X-ray diffraction (WAXD) patterns of the TPU films. The normalized diffraction profiles are vertically offset for clarity and are presented over the 5–40° 2θ range. All formulations exhibited a broad amorphous scattering halo centered at approximately 20–21° 2θ, with no discrete Bragg reflections attributable to well-developed crystalline polymer domains. The overall similarity of the diffraction profiles indicates predominantly amorphous structures with limited long-range molecular ordering across the TPU formulations. Subtle variations in halo width and profile shape suggest only modest formulation-dependent differences in local or short-range structural organization.

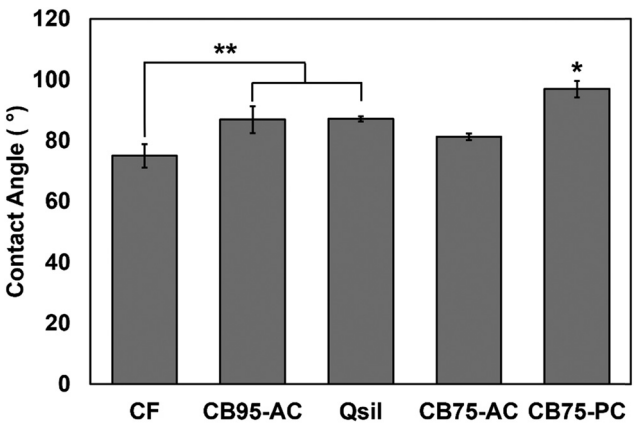


Fig. 8 Contact angle measurements of solution-cast TPU films. All TPU formulations exhibited contact angles within a relatively narrow range, indicating comparable surface wettability. CB75-PC displayed the highest contact angle among all formulations. Values are mean ± SD (n = 3). *Significantly different from other groups, $p < 0.05$, **$p < 0.01$.

thromboplastin time (PTT) values for all materials remained within 80–120% of the control (Fig. 9b), suggesting that the intrinsic coagulation pathway was not measurably altered under the conditions evaluated.

Hemolysis results are presented in Fig. 9c. Most TPU formulations demonstrated negligible hemolytic activity, consistent with good blood compatibility. CB75-AC showed a slightly elevated hemolysis level (~4%), though still relatively low. Representative microtube images corroborate these findings, with non-hemolytic samples displaying clear supernatants, while CB75-AC exhibits a faint increase in red coloration, indicative of mild red blood cell lysis.

3.12. Assessment of a CB95-AC polymeric valve *in vivo*

After implantation, the valve demonstrated persistent moderate mitral regurgitation throughout the 3-week *in vivo* study due to incomplete leaflet coaptation caused by a suture inadvertently looped around one of the valve posts, partially restricting leaflet motion. Despite this mechanical impairment, the valve remained functional and was successfully explanted after 3 weeks of evaluation. Gross examination revealed no evidence of thrombus formation on the leaflet surfaces (Fig. 10a). The small blemish visible on the front leaflet was introduced during sample fixation and handling and is an artifact of specimen preparation rather than an indication of leaflet damage or structural failure occurring *in vivo* (Fig. 10a). Localized fibrin deposition was observed only on the valve annulus adjacent to the restricted leaflet on the atrial side (Fig. 10a). H&E staining demonstrated that the deposit consisted primarily of polymerized fibrin with a small number of entrapped circulating white blood cells (Fig. 10b). Importantly, fibrin deposition was localized to the annular region adjacent to the mechanically restricted leaflet and was not adherent to the TPU leaflet surface itself.

4. Discussion

The performance of thermoplastic polyurethanes (TPUs) as heart valve scaffold materials reflects the combined effects of their segmented architecture, overall formulation, intermolecular interactions, and resulting microphase organization. In this study, systematic comparison of polycarbonate-based and polysiloxane-modified commercial TPU formulations revealed clear formulation-dependent differences in mechanical behavior, oxidative stability, surface characteristics, and hemocompatibility. These differences were interpreted using both manufacturer-reported chemistry classifications and experimentally measured characteristics, including rheological response and FTIR-based carbonyl hydrogen bonding. Accordingly, the present findings establish formulation-level property–performance relationships that are directly relevant to material selection for polymeric heart valve scaffolds. Recent studies of polymeric membrane systems have similarly demonstrated that changes in polymer composition and processing can alter morphology, surface characteristics, mechanical properties, and blood–material interactions, underscoring the interconnected nature of these material attributes.[18–20] Among the materials tested, CB75-AC demonstrated the most favorable elastic recovery and short-term cyclic recovery, while maintaining platelet count and PTT within the predefined acceptance ranges. However, this performance was accompanied by lower tear resistance and slightly elevated hemolysis relative to the other TPU formulations, highlighting the tradeoff between material compliance and mechanical robustness.

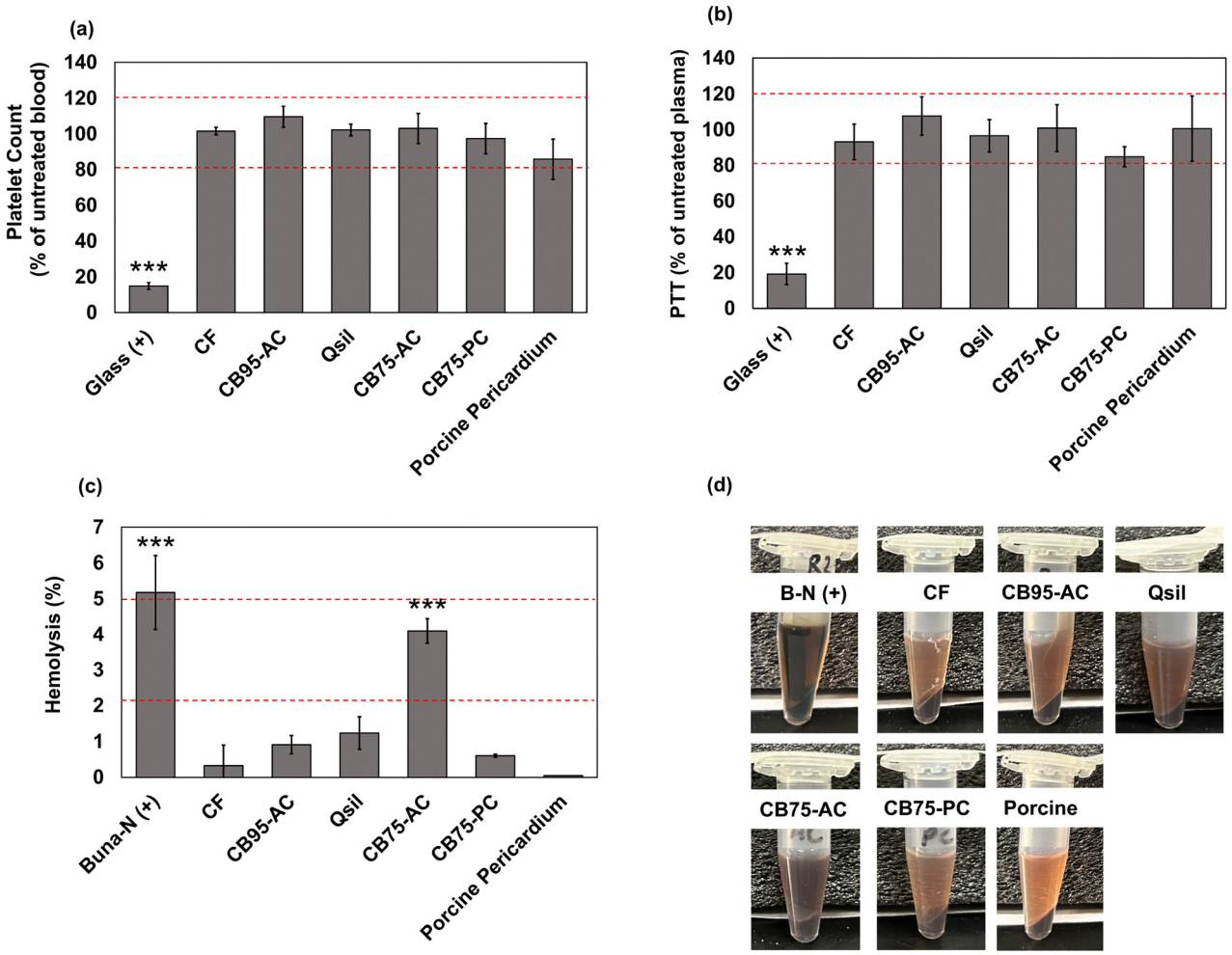


Fig. 9 Hemocompatibility analysis of TPU films. (a) Platelet count normalized to the whole blood negative control, assessed according to ASTM F2888-19. Dashed lines indicate the acceptable range (80–120% of control). All tested TPUs passed the test. (b) Partial thromboplastin time normalized to the plasma negative control, assessed according to ASTM F2382-24. Dashed lines indicate the acceptable range (80–120% of control). All tested TPUs passed the test. (c) Hemolysis (%) evaluated according to ASTM F756-17. Dashed lines indicate classification thresholds. CB75-AC exhibited slight hemolytic activity, while all other TPU samples were classified as non-hemolytic. (d) Representative hemolysis microtubes. Values are mean ± SD (n = 3). ***Significantly different from other groups, $p < 0.001$.

The higher melt viscosity observed in polysiloxane-containing TPUs (Fig. 2a) may reflect stronger intermolecular associations and the formation of a transient supramolecular network within the melt. As deformation frequency increases, these interactions can be progressively disrupted, giving rise to a pronounced shear-thinning response. In polycarbonate-based TPUs, comparatively high melt viscosity may similarly result from the combined effects of intermolecular interactions, molecular entanglement, hard-segment content, and melt-state hydrogen bonding, which together can produce a more elastic and structurally persistent melt.[21] Consistent with these mechanisms, Qsil exhibited the most pronounced shear-thinning, suggesting greater disruption of intermolecular associations with increasing frequency, whereas CB95-AC retained relatively high viscosity at elevated frequencies, consistent with more persistent intermolecular interactions and/or chain entanglements. Among CB75-AC and CB75-PC, the aromatic CB75-AC exhibited higher viscosity than the aliphatic CB75-PC. This difference may be related in part to the greater chain rigidity and intermolecular interactions associated with aromatic segments[22] although other formulation variables may also contribute to the observed rheological behavior. At 20 wt% solution concentration, CB75-AC and Qsil appeared to retain stronger hard-segment associations or aggregate structures, as shown in Fig. 2b, resulting in higher apparent viscosity and moderate shear-thinning. These findings suggest that valve fabrication by dip molding may be more sensitive to dipping and withdrawal speed for CB75-AC and Qsil compared with the other formulations. In contrast, CB95-AC, CF, and CB75-PC exhibited more Newtonian-like behavior, which may reflect improved solvation and reduced intermolecular aggregation under the tested conditions, potentially making these formulations less sensitive to dip-coating speed.[23]

Mechanical performance is a critical determinant of valve durability, as leaflet materials must withstand billions of repetitive loading cycles under physiological conditions

 This journal is © The Royal Society of Chemistry 2026

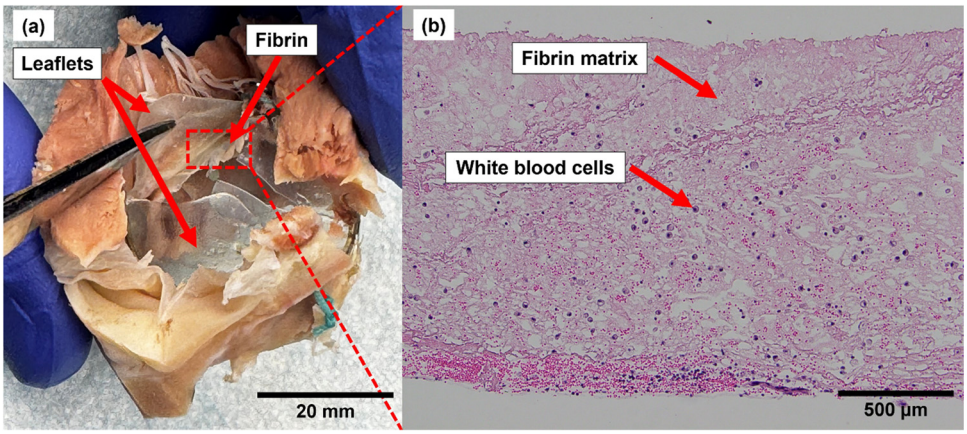


Fig. 10 Gross and histological evaluation of CB95-AC valve after 22 days of implantation. (a) Gross image of the explanted valve demonstrating no thrombus formation on the leaflets and fibrin deposition on valve annulus adjacent to one leaflet with restricted motion. The small blemish visible on the front leaflet was introduced during sample fixation and handling and does not represent leaflet damage or structural failure that occurred *in vivo*. (b) Hematoxylin and eosin (H&E) stained section of the fibrin aggregate demonstrating a polymerized fibrin matrix containing scattered white blood cells.

without structural failure. Tensile testing demonstrated that both stiffness and ultimate strength increased with material hardness, with CF and CB95-AC exhibiting the highest stress-bearing capacities among the tested materials (Fig. 3a). However, for cyclic cardiovascular applications, elastic recovery and resistance to permanent deformation are more critical than peak tensile strength alone. In this regard, CB75-AC exhibited the lowest residual strain and the most efficient elastic recovery during cyclic loading, indicating superior resilience and improved short-term cyclic recovery with reduced permanent deformation under the tested conditions (Fig. 3b). This behavior is consistent with the structure of segmented TPUs, where soft segments provide extensibility and hard segments act as physical crosslinks that stabilize the network.[24] An effective balance between chain mobility and network integrity in CB75-AC may facilitate deformation and recovery, thereby minimizing hysteresis and energy loss during repeated loading.

Under large deformation (50% strain), CB75-AC and CB75-PC exhibited similar residual strain levels, suggesting that at higher strain amplitudes the mechanical response becomes dominated by bulk chain extensibility rather than differences among formulations. Nevertheless, the consistently lower hysteresis and improved recovery of CB75-AC at moderate strain levels are particularly relevant for heart valve applications, where cyclic deformation is frequent. It is also important to note that Qsil exhibited a lower residual strain than CB95-AC (8.9% *vs.* 13.4%, respectively), consistent with the greater elastic behavior observed in Fig. 3b. The effects of oxidative aging further demonstrate formulation-dependent differences in oxidative stability. All materials exhibited some reduction in tensile strength following exposure to hydrogen peroxide (Fig. 3d), consistent with oxidative chain scission mechanisms reported in polyurethane systems.[25] Despite this reduction, polycarbonate-based TPUs generally demonstrate more stable mechanical performance compared to polyether-based counterparts, reflecting their enhanced oxidative resistance.[26] Among the tested materials, CB75-AC exhibited the smallest change in tensile response following accelerated aging, suggesting enhanced resistance to oxidative degradation and better preservation of its microstructural integrity. This stability is particularly important for cardiovascular applications, where materials are continuously exposed to oxidative and inflammatory environments over prolonged periods.

Moisture exposure also altered the mechanical behavior of the TPUs through plasticization effects, as reflected by the increased residual strain observed in wet samples (Fig. 3e). Water uptake disrupts hydrogen bonding interactions between hard and soft segments, thereby increasing polymer chain mobility and reducing material stiffness. This effect was most pronounced in CB95-AC, which exhibited a more pronounced plastic deformation response under wet conditions, whereas CB75-AC, CB75-PC, and Qsil showed comparatively minor changes in mechanical behavior. These findings suggest that certain TPU formulations possess greater resistance to moisture-induced softening, an important consideration for long-term performance in physiological environments. Tear resistance under the three testing conditions—room temperature, wet, and accelerated aging (Fig. 3f) showed that softer polymers are more susceptible to tearing and exhibit lower tear resistance. For polyurethane elastomers, hardness is often correlated with tear resistance because increased hard-segment content and stronger intermolecular interactions improve load transfer and resistance to crack propagation.[27] These findings reveal a balance between tear resistance and elastic recovery in these polymers, where higher tear resistance may be associated with reduced elasticity. The accelerated aging trend for tear is also consistent with the tensile testing results shown in Fig. 3d, where CB75-AC exhibited the smallest reduction in mechanical performance following environmental exposure.

DMA is performed at a very low deformation rate and the results shown in Fig. 4a and b corroborate the tensile testing trends observed in Fig. 3a. The elastic modulus of CB95-AC was higher than that of Qsil. In addition, the lower $\tan\delta$ observed for CB75-AC indicates a more pronounced elastic behavior for

this material, consistent with the tensile and cyclic testing results shown in Fig. 3. The DMA results should be interpreted as comparative material-level viscoelastic data. The selected DMA sweep was not designed to simulate valve function or predict device-level hydrodynamic performance. Instead, it was used to compare storage modulus and damping behavior among the TPU formulations under identical testing conditions. Controlled valve-level hydrodynamic and fatigue studies are required to evaluate functional leaflet performance under physiologic flow and pressure conditions.

Surface chemistry and microphase morphology play a central role in governing biological interactions. FTIR analysis revealed differences in carbonyl bonding states, reflecting variations in urethane carbonyl hydrogen bonding and hard-domain association (Fig. 5). CF exhibited the highest relative hydrogen-bonded carbonyl contribution, whereas CB75-PC exhibited the lowest. These structural differences can be compared to contact angle measurements (Fig. 8), where CB75-PC exhibited the highest hydrophobicity, suggesting preferential surface enrichment of soft segments.[28]

DSC provided complementary evidence of formulation-dependent differences in segmental organization (Fig. 6). CF, which exhibited the highest relative hydrogen-bonded carbonyl contribution by FTIR, also showed a pronounced higher-temperature transition near 145–150 °C, consistent with comparatively thermally persistent hard-segment associations. In contrast, CB75-PC, which exhibited the lowest relative hydrogen-bonded carbonyl contribution, showed a distinct lower-temperature thermal event near 40 °C, consistent with greater segmental mobility and/or weaker hard-domain association. CB75-AC, CB95-AC, and Qsil exhibited broader intermediate-temperature transitions, suggesting distributions of segmental environments rather than well-defined crystalline melting. Taken together, the DSC and FTIR results provide complementary evidence that the TPU formulations possess distinct hard/soft-segment organization and hard-domain association, consistent with their different thermal and mechanical responses.

WAXD provided a complementary assessment of long-range structural order, with all formulations exhibiting broadly similar diffuse scattering profiles centered at approximately 20–21° 2θ and no distinct sharp polymer crystalline reflections (Fig. 7), indicating predominantly amorphous structures with limited long-range crystalline ordering. Similar broad WAXD halos near 20–21° 2θ have been reported for segmented TPUs,[29] including polysiloxane-based systems, and are characteristic of TPU structures with a substantial amorphous contribution.

The hemocompatibility results demonstrate that all TPU formulations maintain platelet counts and PTT values within ASTM-defined acceptable ranges, without substantial platelet consumption or measurable alteration in PTT under the test conditions (Fig. 9). These findings are consistent with previous reports that medical-grade polyurethanes exhibit favorable blood compatibility, largely governed by surface energy, segmental composition, and microphase morphology.[30,31] Protein adsorption and subsequent platelet interactions are known to be strongly influenced by these surface characteristics, which regulate thrombogenic response.[32,33] In the present study, variations in surface wettability and FTIR-derived hydrogen bonding/hard-domain association did not translate into significant differences in platelet or coagulation response, suggesting that all tested materials remained within ASTM-defined acceptable hemocompatibility ranges despite measurable differences in hemolytic response. While most materials exhibited negligible hemolysis, CB75-AC showed a slightly elevated hemolysis level (~4%), placing it within the ''slightly hemolytic'' classification according to ASTM F756-17, although still below the critical threshold. This behavior may be associated with differences in surface chemistry, hard-segment organization, and blood–material interactions. CB75-AC exhibited the lowest stiffness and the highest elastic recovery among the tested materials. The increased segmental mobility of its surface may influence interactions with erythrocyte membranes differently compared with more rigid surfaces. Although such a surface may reduce platelet consumption, as supported by the observed normal platelet count and PTT values, it can permit slightly greater membrane deformation or transient erythrocyte adhesion under dynamic contact conditions, resulting in modest hemolysis. Similar relationships between polyurethane hard-segment structure, surface properties, and blood compatibility have been reported previously in segmented polyurethane biomaterials.[30,31] Importantly, despite its slightly elevated hemolysis, CB75-AC maintained platelet count and PTT within the predefined acceptance ranges under the screening conditions evaluated. These findings highlight the importance of evaluating hemocompatibility using multiple complementary parameters rather than relying on a single assay.[34] Collectively, the results indicate that the TPU films did not cause substantial adverse effects in the screening assays performed under the conditions tested.

Although CB75-AC exhibited the greatest elastic recovery and cyclic stability, it also showed the lowest tear resistance among the TPU formulations evaluated. This limitation is particularly relevant for heart valve applications, where leaflet free edges, commissures, and stent attachment regions are subjected to localized stress concentrations that may promote crack initiation and propagation. Consequently, CB95-AC was selected for preliminary valve fabrication and implantation because its higher tensile strength and tear resistance provided greater structural robustness during device manufacturing, surgical handling, and implantation.

The short-term ovine implantation should be interpreted solely as a preliminary feasibility assessment of the *in vivo* performance of the selected TPU formulation rather than as definitive evidence of long-term valve function. Gross examination after 22 days revealed localized fibrin deposition on the sewing ring adjacent to the leaflet with restricted motion (Fig. 10a), whereas no fibrin deposition, thrombus, or scar tissue was observed on the leaflet surfaces. Although this finding is consistent with the favorable hemocompatibility demonstrated *in vitro*, it should be interpreted with caution. During implantation, one valve post was inadvertently constrained by a suture, resulting in incomplete leaflet coaptation

 This journal is © The Royal Society of Chemistry 2026

and mild mitral regurgitation. This altered the local hemodynamic environment, affecting leaflet kinematics, flow patterns, and blood residence time, all of which can independently influence thrombus and fibrin formation. Therefore, the absence of thrombotic deposition on the leaflet surfaces should be interpreted as an encouraging preliminary observation rather than as definitive evidence of intrinsic antithrombogenicity of the TPU material. Nevertheless, these findings support the feasibility of the selected formulation for further evaluation at the valve level. Future studies using valves with normal leaflet motion under physiologic hemodynamic conditions, together with larger sample sizes and longer implantation periods, will be necessary to further establish material durability and characterize the *in vivo* thrombotic response of the selected formulation.

Moreover, this study focused primarily on acellular TPU films to establish material selection criteria based on mechanical properties, oxidative stability, surface characteristics, and hemocompatibility. These results provide a rational framework for selecting candidate formulations for subsequent development of hybrid tissue-engineered heart valves. Ongoing investigations are evaluating cell adhesion, endothelialization, extracellular matrix deposition, inflammatory responses, and tissue remodeling on selected TPU formulations under physiologically relevant flow and cyclic loading conditions.

Collectively, these findings demonstrate that the performance of TPU-based heart valve scaffolds reflects the combined influence of overall formulation characteristics, intermolecular interactions, microphase organization, and surface properties. Optimization and selection of these materials require balancing elastic recovery, tear resistance, oxidative stability, and hemocompatibility across these interrelated characteristics. These results establish practical formulation–property–performance relationships that can guide the rational selection and further development of PC-TPU materials for future polymeric heart valve scaffolds, including next-generation tissue-engineered heart valve applications.

5. Conclusions

This study identifies formulation-dependent differences in elastic recovery, tear resistance, oxidative stability, thermal behavior, and hemocompatibility among TPU-based heart valve scaffold materials. Softer PC-TPUs showed improved cyclic recovery and lower hysteresis, whereas stiffer formulations provided greater tear resistance and structural robustness. CB75-AC exhibited excellent elastic recovery but limited tear resistance, while CB95-AC provided higher tensile and tear resistance with good elastic recovery and was therefore selected for preliminary valve prototyping and short-term ovine implantation. These *in vivo* findings should be considered preliminary feasibility data. Overall, the results define practical formulation–property–performance criteria for TPU scaffold selection, while further hydrodynamic, fatigue, and long-term implantation studies are needed to establish device-level durability and hemocompatibility.

Conflicts of interest

The authors do not have any conflict of interest.

Data availability

The experimental data presented in this manuscript are available upon any reasonable request.

Acknowledgements

This study was funded by the National Heart, Lung, and Blood Institute (NHLBI) grants: HL153724, HL162687, HL173809, HL177288, and HL157631, as well as the National Science Foundation (NSF) award #2109959.

References

1 J. Butany, M. S. Ahluwalia, C. Munroe, C. Fayet, C. Ahn, P. Blit, C. Kepron, R. J. Cusimano and R. L. Leask, *Cardiovasc. Pathol.*, 2003, **12**, 322–344.
2 D. Bezuidenhout, D. F. Williams and P. Zilla, *Biomaterials*, 2015, **36**, 6–25.
3 P. Zilla, J. Brink, P. Human and D. Bezuidenhout, *Biomaterials*, 2008, **29**, 385–406.
4 S. K. Singh, M. Kachel, E. Castillero, Y. F. Xue, D. Kalfa, G. Ferrari and I. George, *Front. Cardiovasc. Med.*, 2023, **10**, 1137827.
5 A. Vis, B. J. de Kort, W. Szymczyk, J. W. van Rijswijk, S. Dekker, R. Driessen, N. Wijkstra, P. F. Gründeman, H. W. M. Niessen, H. M. Janssen, S. H. M. Söntjens, P. Y. W. Dankers, A. I. P. M. Smits, C. V. C. Bouten and J. Kluin, *Commun. Biol.*, 2023, **6**, 1166.
6 P. B. Zadeh, S. C. Corbett and H. Nayeb-Hashemi, *Mater. Sci. Eng. C*, 2014, **35**, 335–340.
7 D. J. Kereiakes, G. A. Answini, S. J. Yakubov, B. Rai, J. M. Smith, S. Duff, F. L. Shannon, M. Sakwa, J. Beith and D. Heimansohn, *Cardiovasc. Int.*, 2021, **14**, 2754–2756.
8 Q. A. Wang, A. J. McGoron, R. Bianco, Y. Kato, L. Pinchuk and R. T. Schoephoerster, *J. Heart Valve Dis.*, 2010, **19**, 499–505.
9 S. H. Alavi and A. Kheradvar, *Tissue Eng., Part C*, 2011, **18**, 293–301.
10 S. H. Alavi, W. F. Liu and A. Kheradvar, *Ann. Biomed. Eng.*, 2013, **41**, 316–326.
11 S. H. Alavi and A. Kheradvar, *Ann. Thorac. Surg.*, 2015, **99**, 2183–2187.
12 R. Zareian, S. D. Zuke, D. Morisawa, R. S. Geertsema, M. Majid, C. Wynne, J. C. Milliken and A. Kheradvar, *J. Cardiovasc. Dev. Dis.*, 2024, **11**(2), 69.
13 F. Sadeghi, N. Agwu, M. Tacklind and A. Kheradvar, *Ann. Biomed. Eng.*, 2026, DOI: 10.1007/s10439-026-04308-1.
14 F. Sadeghi, Y. Zamani, K. L. Bear and A. Kheradvar, *RSC Adv.*, 2025, **15**, 8839–8850.
15 M. Rashvand and Z. Ranjbar, *Mater. Corros.*, 2014, **65**, 76–81.

16 H. Huang, H. Pang, J. H. Huang, P. T. Yu, J. L. Li, M. G. Lu and B. Liao, *Constr. Build. Mater.*, 2021, **284**, 122388.
17 D. K. Dempsey, C. Carranza, C. P. Chawla, P. Gray, J. H. Eoh, S. Cereceres and E. M. Cosgriff-Hernandez, *J. Biomed. Mater. Res., Part A*, 2014, **102**, 3649–3665.
18 A. Nasir, A. Waseh, T. Ahmad, A. Hussain and F. H. Akhtar, *J. Mater. Chem. B*, 2025, **13**, 13954–13971.
19 M. Zahid, Z. Jahan, M. H. Wadgama, M. B. K. Niazi and F. H. Akhtar, *J. Appl. Polym. Sci.*, 2026, **143**, e70832.
20 B. Qu, Z. Hu, W. Tan, B. Li, Y. Xin, J. Mo, M. Huang, Q. Wu, Y. Li and Y. Wu, *J. Mater. Chem. B*, 2024, **12**, 11810–11816.
21 H. Münstedt, *Soft Matter*, 2011, **7**, 2273–2283.
22 M. Zhou, W. Zhu, S. Yu, Y. Tian, J. Wei and K. Zhou, *J. Micromech. Mol. Phys.*, 2023, **8**, 11–24.
23 C. L. de Vasconcelos, R. R. Martins, M. O. Ferreira, M. R. Pereira and J. L. C. Fonseca, *Polym. Int.*, 2002, **51**, 69–74.
24 G. Scetta, J. Z. Ju, N. Selles, P. Heuillet, M. Ciccotti and C. Creton, *J. Polym. Sci.*, 2021, **59**, 685–696.
25 G. F. Meijs, S. J. Mccarthy, E. Rizzardo, Y. C. Chen, R. C. Chatelier, A. Brandwood and K. Schindhelm, *J. Biomed. Mater. Res.*, 1993, **27**, 345–356.
26 E. M. Christenson, J. M. Anderson and A. Hiltner, *J. Biomed. Mater. Res. A*, 2004, **70a**, 245–255.
27 X. Jin, N. S. Guo, Z. P. You and Y. Q. Tan, *Materials*, 2020, **13**, 4991.
28 S. Naheed, M. Zuber, M. Salman, N. Rasool, Z. Siddique, M. R. Shaik, M. A. F. Sharaf, A. Abdelgawad, D. Sekou and E. M. Awwad, *Polymers*, 2021, **13**, 2060.
29 W. C. Wang, X. Y. Bai, S. A. Sun, Y. Y. Gao, F. Z. Li and S. K. Hu, *Int. J. Mol. Sci.*, 2022, 23.
30 L. Nguyen, L.-C. Xu, E. Yeager, W. J. Weiss and C. A. Siedlecki, *J. Biomater. Appl.*, 2023, **38**, 302–310.
31 Y. Hu, Y. Xiong, Y. Wei, J. Liu, T. Zheng, C. Zheng, G. Li, R. Luo, L. Yang and F. Zhang, *Acta Biomater.*, 2024, **190**, 64–78.
32 Z. Riedelová, A. de los Santos Pereira, J. Svoboda, O. Pop-Georgievski, P. Májek, K. Pečánková, F. Dyčka, C. Rodriguez-Emmenegger and T. Riedel, *Macromol. Biosci.*, 2022, **22**, 2200247.
33 L. C. Xu and C. A. Siedlecki, *J. Biomed. Mater. Res. B*, 2017, **105**, 668–678.
34 J. P. Santerre, K. Woodhouse, G. Laroche and R. S. Labow, *Biomaterials*, 2005, **26**, 7457–7470.

 This journal is © The Royal Society of Chemistry 2026